

# Tidal dwarf candidates in a sample of interacting galaxies<sup>\*,\*\*</sup>

P.M. Weilbacher<sup>1</sup>, P.-A. Duc<sup>2,3</sup>, U. Fritze von Alvensleben<sup>1</sup>, P. Martin<sup>4</sup>, and K.J. Fricke<sup>1</sup>

<sup>1</sup> Universitätssternwarte, Geismarlandstrasse 11, 37083 Göttingen, Germany

<sup>2</sup> CNRS URA 2052 and CEA, DSM, DAPNIA, Service d'Astrophysique, Centre d'Etudes de Saclay, 91191 Gif-sur-Yvette Cedex, France

<sup>3</sup> Institute of Astronomy, University of Cambridge, Madingley Road, Cambridge, CB3 0HA, UK

<sup>4</sup> Canada-France-Hawaii Telescope, P.O. Box 1597, Kamuela, HI 96743, USA

Received 30 July 1999 / Accepted 28 March 2000

**Abstract.** We present deep optical  $B, V, R$  images of a sample of 10 interacting systems which were selected for their resemblance to disturbed galaxies at high redshift. Photometry is performed on knots in the tidal features of the galaxies. We calculate a grid of evolutionary synthesis models with two metallicities and various burst strengths for systems consisting of some fraction of the stellar population of a progenitor spiral plus starburst. By comparison with two-color diagrams we interpret the photometric data, select from a total of about 100 condensations 36 star-forming objects that are located in the tidal features and predict their further evolution. Being more luminous by 4 mag than normal H II regions we argue that these objects could be tidal dwarf galaxies or their progenitors, although they differ in number and mean luminosity from the already known tidal dwarf galaxies typically located at the end of tidal tails in nearby giant interacting systems. From comparison with our models we note that all objects show young burst ages. The young stellar component formed in these tidal dwarf candidates contributes up to 18% to the total stellar mass at the end of the starburst and dominates the optical luminosity. This may result in fading by up to 2.5 mag in  $B$  during the next 200 Myrs after the burst.

**Key words:** galaxies: formation – galaxies: interactions – galaxies: photometry – galaxies: evolution

## 1. Introduction

Most investigations of interacting and merging galaxies have essentially focussed on the phenomena occurring in their inner regions. However, for a few spectacular cases like the Antennae (Mirabel et al. 1991), Arp 105 (Duc & Mirabel 1994; Duc et al. 1997) and NGC 7252 (Hibbard & Mihos 1995) the enormous tidal tails were investigated in some detail. Massive condensations of stars and H I were found in these tails, the so called Tidal Dwarf Galaxies (TDGs).

*Send offprint requests to:* P. Weilbacher (weilbach@uni-sw.gwdg.de)

\* Based on observations collected at the European Southern Observatory, La Silla, Chile (ESO No 058.A-0260).

\*\* Tables 5–14 are only available in electronic form at the CDS via anonymous ftp to 130.79.128.5 or via <http://cds.u-strasbg.fr/Abstract.html>

TDGs are characterized by a luminosity comparable with that of typical dwarf galaxies, but which span a range in oxygen abundance of  $8.3 \lesssim 12 + \log(O/H) \lesssim 8.6$  equivalent to metallicities of  $4 \cdot 10^{-3} \lesssim Z_{\text{TDG}} \lesssim 8 \cdot 10^{-3}$  with a mean of  $Z \approx 7 \cdot 10^{-3} \approx Z_{\odot}/2.6$ .<sup>1</sup> Metallicities of TDGs are therefore higher than those of other dwarf galaxies with comparable luminosity (Duc & Mirabel 1997, 1998). TDGs have blue colors as a result of an active starburst. Most known TDGs have high H I masses from which total masses of the order of  $10^9 M_{\odot}$  have been estimated. They are gravitationally bound and in a few interacting systems evidence for their kinematical independence has been found (e.g. Duc et al. 1997; Duc & Mirabel 1998). These systems together with the strong increase of the galaxy merger rate with redshift gave rise to speculations about a possible contribution of TDGs to the faint blue galaxy excess at high redshift (Fritze-v. Alvensleben et al. 1998). Barnes & Hernquist (1992) observed the formation of TDGs in their numerical simulations. Their 3D N-body/SPH-code created several massive bound condensations along the tidal tails. At first, their mass is dominated by the stellar component. Later on, gas from the tail might fall into these condensations. Elmegreen et al. (1993) proposed a different scenario. They have used a 2D N-body code including dissipation for the gas component in which gaseous condensations form first.

Observations in most cases show both components, neutral gas and stars, along the tails as well as in their condensations. In an optically identified condensation, determination of the relative fraction of young stars – born in situ from the collapse of tidally extracted H I – to old stars – pulled out from the progenitor disk(s) – might constrain the above mentioned numerical models. Because the systems studied here are too distant to be resolved into stars, estimating these relative stellar fractions can only be done from multi-band integrated photometric measurements in comparison with an evolutionary synthesis model. Photometric work on the tidal features of several classical interacting systems has been carried out by Schombert et al. (1990). Studies by

---

<sup>1</sup> For metallicity we use the notation of  $Z$  (as the proportion of heavy elements given in the Geneva stellar tracks which our models are based on) throughout this paper and give a comparison with the solar value  $Z_{\odot} = 0.018$  where appropriate.

**Table 1.** Observation log

Field No.	Object	Observing Date	Seeing ["]	total Exposure Time [s]		
				<i>B</i>	<i>V</i>	<i>R</i>
1	AM 0529-565	02./03.03.97	0.8	2400	1800	1800
2	AM 0537-292	28.02.97	0.9	1200	900	900
3	AM 0547-244	01.03.97	1.1	1200	900	900
4	AM 0607-444	03.03.97	0.8	1200	900	900
5	AM 0642-645	08.04.97	1.3	1200	900	900
6	AM 0748-665	16.03./03.04.97, 10.04.96	1.1	3600	3000	3000
7	AM 1054-325	11.04.	0.8	1200	900	900
8	AM 1208-273	03.04.97	1.0	1200	900	900
9	AM 1325-292	03.04.97	0.9	1200	900	900
10	AM 1353-272	15./16.03.97	0.8	2400	1200	1200

Appleton & Marston (1997) and Bransford et al. (1998) concentrated on ring galaxies. Deeg et al. (1998) have systematically catalogued all faint non-stellar objects around disturbed galaxies. Part of them might be TDG candidates.

These previous investigations have focused on disk-disk interacting systems with a well-understood morphology, e.g. well defined tails. However locally the majority of disturbed galaxy systems, for instance in the Catalogue of Southern Peculiar Galaxies (Arp & Madore 1987), do not have long tails. In particular disk-spheroid collisions and 3-body systems leading to chaotic morphologies are quite common. HST deep surveys with the WFPC2 show that the percentage of disturbed (i.e. interacting, merging or peculiar) galaxies has been much higher in the early universe than today (van den Bergh et al. 1996). NICMOS observations in the near-infrared have shown that these disturbances are not only due to irregularities in the distribution of star forming regions, but reflect real morphological features of interactions (Conselice et al. 1998). These galaxies at high redshift often do not show long tidal tails either because they are absent or because they have too low a surface brightness. Examining a local sample which resembles these high redshift interacting galaxies is therefore important to learn about their evolution.

In this paper we extend previous investigations of a few individual systems to deep optical photometry of a sample of peculiar galaxies. The objects from our sample mostly do not possess prominent tidal tails, but definitely show signs of merging, as e.g. multiple nuclei or disturbed morphology and nearby companions. The sample is extracted from the Catalogue of Southern Peculiar Galaxies (Arp & Madore 1987). It includes disk-disk, disk-elliptical, dwarf-dwarf and 3-body systems observed at different stages of the interaction.

Spectrophotometric evolutionary synthesis models have been used for various applications of normal galaxy evolution. More recently starburst events were modeled as well. These models assume that the standard star-formation rate (SFR) of an underlying galaxy is increased to simulate a starburst (Fritze-v. Alvensleben & Gerhard 1994a; Leitherer & Heckman 1995). This technique has been applied to reproduce the star formation history of various classes of objects from merging galaxies

(Fritze-v. Alvensleben & Gerhard 1994b) to blue compact galaxies (Krüger et al. 1995).

We take an approach similar to the latter and compute a grid of models specifically aimed to describe the properties found in previous investigations of TDGs. We do not use solar-abundance tracks in our models but instead two more realistic metallicities in the range expected for TDGs ( $Z = 1 \cdot 10^{-3}, 8 \cdot 10^{-3}$ ). As a primary goal, these models are used to select candidate TDGs or TDG progenitors. Based on their colors only, background objects can be excluded not only with statistical methods but also one by one if they disagree with any kind of TDG model. Furthermore, this technique allows to derive the present ratios of old to young stellar mass in these TDG candidates, to predict its evolution and hence to constrain the above-mentioned formation scenarios of TDGs. Obviously spectrophotometric data is required to confirm the photometric results.

The structure of the paper is as follows. First we present our data reduction and analysis techniques (Sect. 2). We describe in Sect. 3 the evolutionary synthesis models and the parameters used to interpret the photometric data. In Sect. 4 we present our sample, compare with the model grid and comment on individual features of the interacting systems. In Sect. 5 we discuss more general results and in particular compare the tidal objects identified in our sample with those produced in numerical models and with the few typical TDGs studied so far.

## 2. Observations and data reduction

### 2.1. Data and calibration

Optical *B,V,R* images of 10 galaxies were obtained in visitor mode on April 10th, 1996 and in service mode from February to April 1997 using SUSI on the NTT. The SUSI camera has a field of view of  $2'2 \times 2'2$  and a pixel scale of  $0''.13$ . The objects of our sample with observing dates, seeing conditions and total exposure times are given in Table 1.

The data reduction was performed in IRAF using the CCDRED package with the classical procedures of bias-subtraction and flat-fielding. In order to correct the sky background for some residuals we constructed illumination frames by modeling the background fitted at positions not contaminated by object light. Cosmic ray hits were removed using COSMICRAYS. The images

in all filters were then registered and PSF-matched using several reference stars. Foreground stars were, when possible, deleted and replaced by a background fit using the IMEDIT task.

Standard stars from the fields of Landolt (1992) have been used to derive the zeropoints and estimate the color terms. The extinction coefficients were taken from the La Silla extinction database provided by the Geneva group (e.g. Burki et al. 1995). With this data we could derive a photometric calibration accurate to about 0.04 mag for most targets. One should note that most of the observations were obtained during the refurbishment of the NTT and that the standard stars have not always been observed during the same night as the science targets. Therefore additional systematic calibration errors cannot be excluded; however, our zeropoints and color terms appear to be very stable from one night to the other. Their variations are smaller than 0.01 mag i.e. smaller than the given errors. Except for a few cases for which the extinction given by the Geneva group has large uncertainties, high calibration errors might be present (e.g. AM 0607-444). Figs. 3 to 23 in Sect. 4 show  $1\sigma$ -errorbars for the systematic error for each field due to uncertain calibration and individual errors for each object due to photon statistics and background noise.

We also obtained longslit-spectra of AM 0529-565, AM 1325-292, and AM 1353-272 using EMMI at the NTT in May 1998. The reduction was performed in the standard way and the spectra were used to measure the redshift. Further details will be given in a forthcoming paper.

## 2.2. Aperture photometry

As the features of interest within the tidal debris are irregular in shape and located in regions with high and irregular background, traditional photometry with circular apertures was not appropriate since it would have included too much flux from the surrounding tidal features. We therefore developed a reproducible technique to analyze these knots using polygonal apertures and used circular apertures only for objects far away from the main body of the interacting system.

The  $V$ -band intensity scale of each image was transformed to calibrated surface brightness and contour plots were created of the interesting regions of each frame. The objects to measure were selected from the most prominent peaks in surface brightness. Polygonal apertures were then defined following the faintest contour which still allows separating the knot from surrounding tidal features. The surface brightness level  $\mu_V$  of the aperture was therefore different for each knot and is given in Tables 5 to 14<sup>2</sup>. The sky flux was individually measured at several positions nearby each knot, carefully avoiding the tidal features, and averaged. We are interested in both the young and the old stellar population which the (stellar) tail consists of, because we explicitly model the old population in our evolutionary synthesis models. Hence we only subtract the sky background but not the tidal tail from the object flux. The photometry was finally performed using the IRAF POLYPHOT task with the same

polygonal aperture for all photometric bands. Tables 5 to 14 give the complete photometric results. Column 1 gives the identification, column 2 the surface brightness  $\mu_V$  of the polygonal aperture. Columns 3 to 5 show the apparent magnitudes in  $B$ ,  $V$  and  $R$ , while columns 6 to 8 present the optical colors  $B - V$ ,  $V - R$  and  $B - R$ . Columns 9 to 11 show the photometric errors of the measurements in  $B$ ,  $V$  and  $R$ . All given magnitudes and colors are corrected for galactic extinction, using the  $A_B$  values of Burstein & Heiles (1982) and extrapolating to  $V$  and  $R$  with the ratios of Savage & Mathis (1979).

## 3. Model

### 3.1. Modelling the old population

Spectrophotometric and chemical evolutionary synthesis models are used to interpret the photometric data. Our code is based on the work of Krüger (1992) which was originally used to model BCDGs (Krüger et al. 1995). To include the underlying old component in our model, it starts with a gas cloud of primordial metallicity and follows the evolution of ISM abundances and spectrophotometric properties of the stellar population of an undisturbed galaxy until the starburst induced by the interaction occurs. The model includes the two basic parameters, star formation rate (SFR)  $\psi(t)$  and initial mass function (IMF). We use SFRs proportional to the gas to total mass ratio for Sb and Sc models and a constant SFR for Sd with efficiencies appropriate for the respective galaxy types (see e.g. Fritze-v. Alvensleben & Gerhard 1994a).

As our observations cannot constrain the IMF, we use the IMF from Scalo (1986) in the mass range 0.15 to 120  $M_\odot$  and, for simplicity, assume the same IMF for the progenitor spiral and the starburst. To cover a Hubble time of evolution for the undisturbed progenitor spiral and have a good time resolution during and after the burst, we use a variable timestep as outlined by Krüger (1992).

### 3.2. Input physics

The model uses Geneva stellar evolutionary tracks (Schaller et al. 1992; Charbonnel et al. 1993; Schaerer et al. 1993a,b; Charbonnel et al. 1996). We present models for two different metallicities  $Z_1 = 1 \cdot 10^{-3} \approx Z_\odot/18$  and  $Z_3 = 8 \cdot 10^{-3} \approx Z_\odot/2.3$ .

As shown by Krüger et al. (1995) the broadband colors are dominated by nebular line and continuum emission in the early phases of a strong burst. We therefore include nebular emission in our models using the compilation from Schaerer & de Koter (1997) to calculate the number of Lyman continuum photons emitted per second  $N_{\text{Lyc}}$  of our stellar population as a function of time. With the standard formula

$$F(\text{H}_\beta) = 4.757 \cdot 10^{-13} f N_{\text{Lyc}} \text{ergs}^{-1}$$

we obtain the  $\text{H}_\beta$ -flux. Fluxes of the other hydrogen lines are computed from their line ratios relative to  $\text{H}_\beta$ .  $f$  is the proportion of Lyman continuum photons not absorbed in dust. We take  $f = 1.0$  for  $Z_1$  and  $f = 0.7$  for  $Z_3$ .

<sup>2</sup> Tables 5 to 14 are available only in electronic form.

**Table 2.** Set of model parameters.

Run ID	$\tau_B$ [yr]	$\psi_0$ [ $M_\odot \text{ yr}^{-1}$ ]	$b$	$L_{\text{young}}/L_{\text{tot}}$ $B$	$L_{\text{young}}/L_{\text{tot}}$ $R$
1	$5 \cdot 10^5$	100	0.01	0.56	0.37
2	$5 \cdot 10^5$	500	0.05	0.87	0.75
3	$5 \cdot 10^5$	1000	0.10	0.93	0.85
4	$1 \cdot 10^6$	100	0.02	0.69	0.49
5	$1 \cdot 10^6$	500	0.09	0.92	0.83
6	$1 \cdot 10^6$	1000	0.18	0.96	0.91
7	$5 \cdot 10^6$	50	0.04	0.76	0.58

To include other typical lines of star-forming regions we use the observed line ratios of 27 lines in the wavelength range from 1335 to 10330 Å from Izotov et al. (1994) for low metallicity ( $Z_1$ ) and theoretical line ratios from Stasińska (1984) for medium metallicity ( $Z_3$ ) models.

We chose to use the metallicities  $Z_1$  and  $Z_3$  given above<sup>3</sup>. In the context of comparing our models to observed objects these metallicities should not be regarded as fixed values, but more as metallicity ranges,  $Z_1$  as  $0.001 < Z < 0.006$  and  $Z_3$  as  $0.006 < Z < 0.012$ .

### 3.3. TDG models

To model both the star-forming young and the old component of a TDG with our 1-zone model, we let a typical part of a disk galaxy evolve with its appropriate SFR over 13 Gyrs. After 13 Gyrs a starburst is assumed to occur (triggered by an interaction) in this part of the model galaxy assumed to form a TDG. In the burst the SFR is set to a maximum value  $\psi_0$  and decreases exponentially with a timescale  $\tau_B$ .

The time of the starburst is inferred from a rough age of present-day galaxies of 14 Gyr in a reasonable cosmological model. We look back roughly 1 Gyr, the assumed epoch for the starburst following an interaction. The model is followed for another 3 Gyrs after the burst. The galaxy age at the onset of the burst does not significantly change the color evolution during or after the burst.

According to previous observations the model with metallicity of  $Z_3$  should a priori best apply to TDGs. In the dynamical formation scenarios of Barnes & Hernquist (1992) and Elmegreen et al. (1993), TDGs are predicted to form out of material from the outer parts of the progenitor or from the progenitor galaxy disks. This material in nearby galaxies has a metallicity of  $Z \approx 7 \cdot 10^{-3} \approx Z_3$  (Zaritsky et al. 1994; Ferguson et al. 1998). Indeed, spectroscopy of TDGs confirms this mean metallicity (Duc & Mirabel 1997, 1998). However, the precise metallicity expected for a particular condensation depends on the type and luminosity of the progenitor galaxy – late type and low luminosity spirals being more metal poor on average than earlier type or higher luminosity spirals – and on

<sup>3</sup> Another possible metallicity given in the Geneva stellar tracks ( $Z_2 = 4 \cdot 10^{-3}$ ) is not used in our models because no emission line ratios are available for it.

the region of the parent galaxies where this particular material is torn out from, since galaxies tend to have negative abundance gradients in stars and the gas with increasing radius. Both at higher redshift in general and in the local universe in those cases where dwarf or very low metallicity galaxies are involved in the encounter, TDGs with lower metallicity might also form. However, the recycled nature of TDGs precludes metallicities lower than about 1/20 solar. Models with  $Z_1$  predict that they should populate distinctly different regions in optical color-color diagrams, i.e. have very blue  $V - R$  at moderately blue  $B - V$ . Models with  $Z_1$  have been applied in those cases.

To produce the various proportions of old and young populations observed in TDGs, the maximum SFR and the timescale of the burst  $\tau_B$  are varied. The resulting burst strength  $b$  is computed as the ratio of the mass of stars formed during the burst and the total mass of stars ever formed in the galaxy. Our model grid is presented in Table 2. Column 1 gives a code for each model, which is used in the plots in Sect. 4 together with the metallicity. Columns 2 and 3 give the max. SFR and decay time of the burst and column 4 the burst strength. Columns 5 and 6 give the relative contributions of the starburst component to the luminosities in the  $B$  and  $R$  bands.

### 3.4. Model application and limitations

We discuss here the application and limitations of our grid of models to derive the properties of the observed condensations in the tidal features. Fig. 1a details the track in a  $B - V$  vs.  $V - R$  two-color diagram for one given burst-model and various assumptions for the underlying parent galaxy. The color evolution is plotted from the start of the burst at 13 Gyrs (underlying galaxy Sd) when a subpopulation of the progenitor spiral is expelled into a tidal tail and begins to form a TDG. With the burst, the colors become bluer, at first most noticeable in  $V - R$  and then in  $B - V$  when the starburst begins to fade. In the two-color diagram this color evolution produces a loop which is followed counterclockwise. While the color evolution is very rapid at the beginning of the burst, it slows down considerably as the burst ages. The type of the underlying galaxy and hence its star formation history slightly affect the starting point of the loop but do not significantly change its shape. Due to lack of detailed knowledge of the spectral type of the undisturbed progenitor we choose to uniformly model the old population with a constant SFR.

Figs. 1b and c display the curves of all models that have been probed for the two metallicities  $Z_1$  and  $Z_3$ , respectively. It can be seen that a higher initial burst SFR  $\psi_0$  and hence a higher burst strength  $b$  produces a larger loop. The different shapes of the loops for models with equal strength but different metallicities is mainly caused by the varying fluxes of the emission lines which strongly contribute to the optical broad band colors during the burst (Krüger 1992).

The dots plotted in Fig. 1 show five representative artificial data points chosen to demonstrate in howfar the various properties of a burst can be disentangled using two colors only. Data point “1” lies in a region in the two-color plane which can only

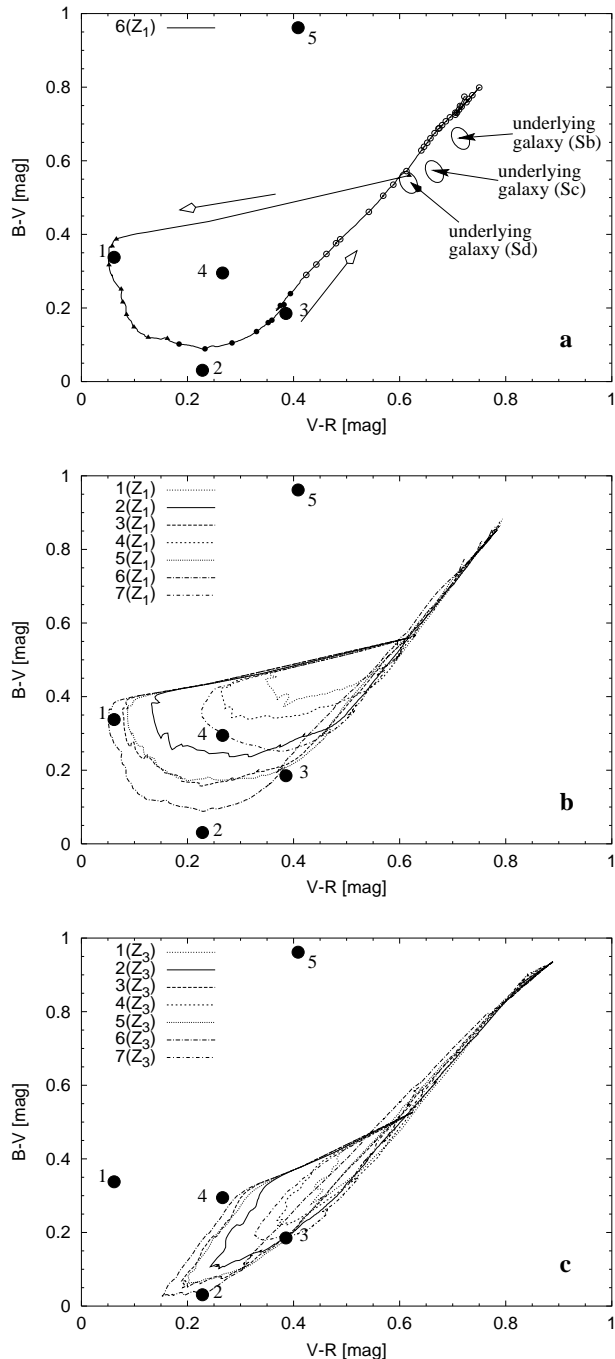


**Fig. 1a–c.** Examples of model curves in a  $B - V$  vs.  $V - R$  diagram for various burst parameters. Five “data points” are shown as examples, see discussion in the text. **a** shows the strongest low metallicity burst model with tick marks indicating the burst age: The triangles are separated by 1 Myr starting at the onset of the burst, the filled circles are separated by 10 Myrs, and the open circles by 100 Myrs. **b** shows all low metallicity ( $Z_1$ ) burst loops and **c** all medium metallicity bursts.

be reached by a low metallicity model with high burst strength ( $b > 0.1$ ) and young burst age (about 2.5 Myrs). Data point “2” needs a high burst strength ( $b > 0.1$ ) and medium burst age (around 20 Myrs), whatever the metallicity, the medium metallicity model providing a better match. Data point “3” is more

ambiguous with respect to the metallicity but clearly needs a much higher age (above 80 Myrs) and a medium to strong burst ( $b > 0.05$ ). Depending on the metallicity data point “4” can be either an intermediate strength burst (low  $Z$ ,  $0.02 < b < 0.05$ , young age  $\approx 1$  Myr) or strong burst (for medium  $Z$ ,  $b > 0.10$ , age  $\approx 7$  Myrs). Additional colors or spectroscopy are needed to resolve the ambiguity. Data point “5” does not agree at all with any of our models. Its colors are indicative of a redshifted background galaxy (see Sect. 5.1 and Möller et al. in prep.).

In Sect. 4 we compare the photometry of the star-forming knots lying in or close to the tidal features of our interacting galaxies with predictions of various TDG models. The primary goal is to isolate objects consistent with a TDG scenario from background sources. A metallicity of  $Z_3$  as observed for TDGs was a priori selected unless other indicators (a metallicity measurement from spectroscopic data, the luminosity class of the parent galaxy, or colors that clearly indicate a low metallicity model like data point “1”) favor a  $Z_1$  model. The burst parameters were determined by visual comparison of the position of the data points to the model curves. The model with the smallest deviation from an observed data point was selected as “most likely” model from our grid. We can also assess which other models represent a reasonable match within the observational uncertainties and from that derive likely ranges for the burst age and strength of any tidal object (see Table 4). Given the individual and systematic photometric errors and the two-dimensional nature of the data, a numerical fitting routine did not seem to be warranted.

As the modelling of the undisturbed galaxy is created for an average late-type galaxy the colors of the nuclei or the parent galaxies plotted in Sect. 4 may have strongly differing colors (as in the case of AM 1325-292, see Fig. 20). This does not affect the validity of our models with respect to the TDG candidates.

It should be noted that the comparison of observation with models only relies on the two colors  $B - V$  and  $V - R$ . To account for the effect of dust obscuration on the colors, a larger set of photometric data including the NIR regime or spectral information would be needed. In the following, we neglect any internal extinction. The effect of  $A_B = 0.5$  mag absorption is indicated by an arrow in the plots in Sect. 4. A significant extinction (of e.g.  $A_B = 0.5$  mag or more) would therefore result in underestimating the burst strength, but would not change the final conclusions drawn from the model.

## 4. Results

Figs. 2 to 21 present surface brightness images of all the systems in our sample and the two-color diagrams for comparison with the evolutionary synthesis models. The objects of interest are identified on the charts and the plots. The principal objects – those that most probably pre-existed the interaction – have been labeled with capital letters, while the smaller features – those that are TDG candidates – have small letters. An overview of the properties of all parent galaxies is given in Table 3. The properties of the objects for which we have inferred a tidal origin and are good candidates for TDGs or their progenitors are listed

**Table 3.** Properties of the parent galaxies.

Name	Velocity [km s <sup>-1</sup> ]	<i>B</i> [mag]	<i>M<sub>B</sub></i> <sup>1</sup> [mag]	Morphology
AM 0529-565 A	4420 <sup>5</sup>	15.83	-18.3	Merger
AM 0529-565 D	4645 <sup>5</sup>	18.46	-15.4	dI
AM 0537-292 A	–	14.97	–	Sb? <sup>2</sup>
AM 0537-292 B	–	16.56	–	E
AM 0547-244 A	13164 <sup>3</sup>	15.62	-20.6	S pec
AM 0547-244 B	–	17.10	–	S?
AM 0607-444 A	–	15.36	–	Sc:pec
AM 0642-645 A	–	16.44	–	Pec
AM 0748-665 A	–	18.01	–	S
AM 0748-665 B	–	16.37	–	E
AM 1054-325 A	3795 <sup>4</sup>	14.55	-19.0	Sm
AM 1054-325 B	–	15.31	–	S pec
AM 1208-273 A	14778 <sup>3</sup>	15.62	-20.9	Sc <sup>2</sup>
AM 1208-273 B	12433 <sup>3</sup>	16.28	-19.8	Pec
AM 1325-292 A	4598 <sup>5</sup>	13.90	-19.9	SB(s)b <sup>2</sup>
AM 1325-292 B	4431 <sup>5</sup>	13.43	-20.4	E1 pec <sup>2</sup>
AM 1353-272 A	11791 <sup>5</sup>	15.77	-20.3	Sc:pec
AM 1353-272 B	12145 <sup>5</sup>	17.96	-18.1	S pec

<sup>1</sup> We use  $H_0 = 75 \text{ km s}^{-1}$  throughout this paper

<sup>2</sup> The morphological type was taken from NED

<sup>3</sup> from Donzelli & Pastoriza (1997)

<sup>4</sup> from Sekiguchi & Wolstencroft (1993)

<sup>5</sup> from Weilbacher et al. 2000 in prep.

in Table 4. The model curves shown on the diagrams are those representing a maximum number of data points.

#### 4.1. AM 0529-565

The image of this system at a redshift of  $V_A = 4420 \text{ km s}^{-1}$  is shown in Fig. 2. The principal galaxy, “A”, has an integrated absolute blue magnitude typical of a Magellanic Irregular galaxy. However the presence of a double nucleus and of diffuse tidal tails are characteristics of mergers. The eastern nucleus “Ae” has redder colors than the western one “Aw” which is currently in a starburst phase (see Fig. 3). “B” is an elliptical galaxy. Given its colors, it is probably a background object with an estimated redshift of  $\approx 0.2$  (Möller et al. in prep.). “C” is a peculiar low surface brightness (LSB) galaxy of unknown redshift. “D” is a blue dwarf galaxy associated with “A” at a relative velocity of  $V_{\text{rel}} = 220 \text{ km s}^{-1}$ . Several diffuse knots can be seen around “A”; they are designated with “a” to “l”. “a” seems to be detached from the eastern tidal tail.

From preliminary spectroscopic test observations of AM 0529-565 (Weilbacher et al. 2000, in prep.), we could estimate an oxygen abundance of  $12 + \log(O/H) = 8.1$  (equivalent to  $Z = 0.003$ ) for “e” and “h” and a very low  $12 + \log(O/H) = 7.6$  (equiv. to  $Z = 0.0008$ ) for object “D”. Because of its much smaller metallicity, “D” is most probably a pre-existing galaxy currently in interaction with “A”.

Fig. 3 shows that the colors of most of the knots in the tidal debris are consistent with TDG burst models with low metallicity ( $Z_1$ ) and burst strength in the range  $0.02 < b < 0.18$ .

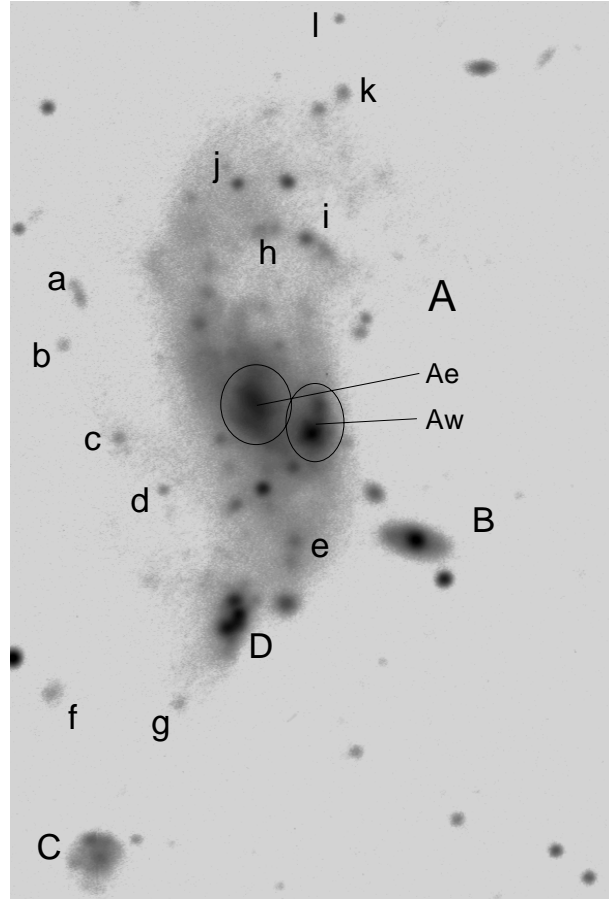


**Fig. 2.** Identification chart of field 1 around AM 0529-565.

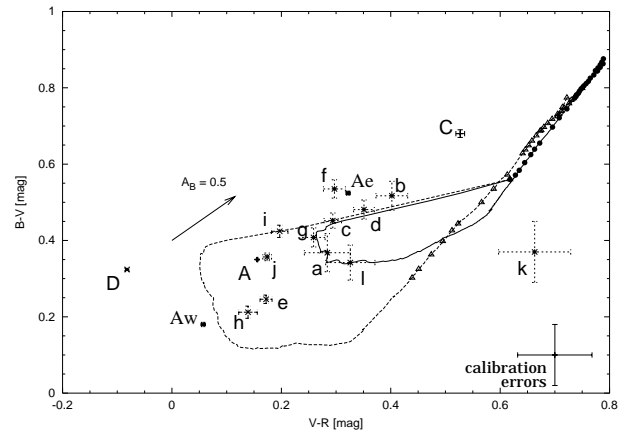


**Fig. 3.** Plot of the objects in field 1 of AM 0529-565. The models used are  $4(Z_1)$  (solid,  $b = 0.02$ ) and  $6(Z_1)$  (dashed,  $b = 0.18$ ).

#### 4.2. AM 0537-292

The image of this system also known as MCG-5-14-9 is shown in Fig. 4. “A” is a strongly disturbed galaxy with tidal tails and a central bar. “B” has the morphology of an E5 galaxy in the central part, but the contours get distorted further out. The overall color of both galaxies is strongly dominated by the light of the

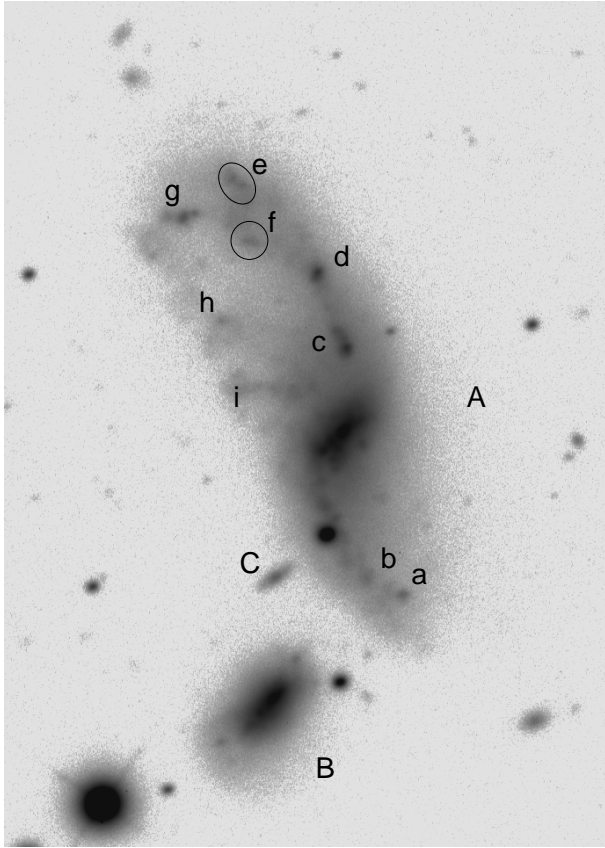


**Fig. 4.** Identification chart of field 2 around AM 0537-292.

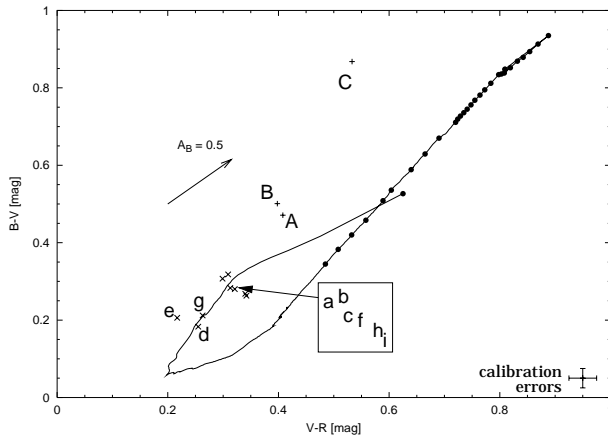


**Fig. 5.** Plot of the objects in field 2 of AM 0537-292. The model used is  $5(Z_3)$  (solid) with  $b = 0.09$ .

nuclei. “C” and all other unnamed visible extended objects in the field are found to be background galaxies from their colors.

Several large blue knots probably associated with star-forming regions can be seen in the tails. They are labeled “a” to “i”. Fig. 5 shows that all knots are well described by the  $Z_3$  model with a burst strength of the order of 10%. They have similar burst ages of around 3 Myrs.

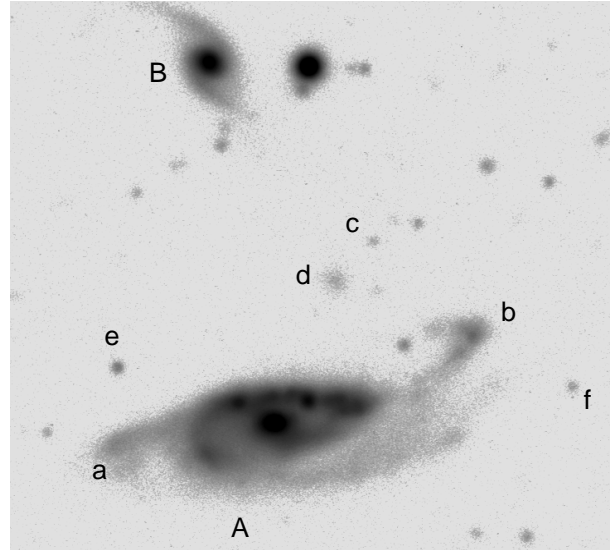


**Fig. 6.** Identification chart of field 3 around AM 0547-244.

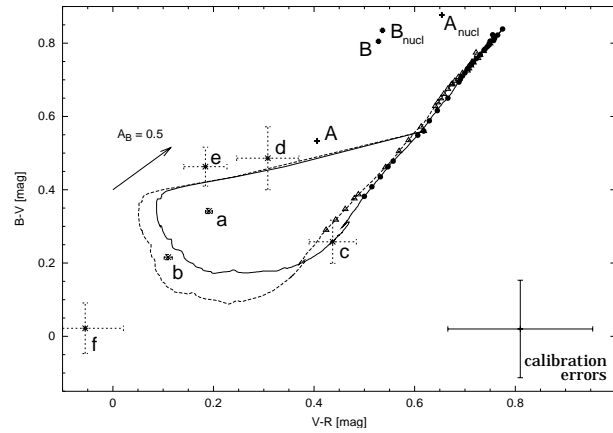


**Fig. 7.** Plot of the objects in field 3 of AM 0547-244. The models used are  $5(Z_1)$  (solid,  $b = 0.09$ ) and  $6(Z_1)$  (dotted,  $b = 0.18$ ).

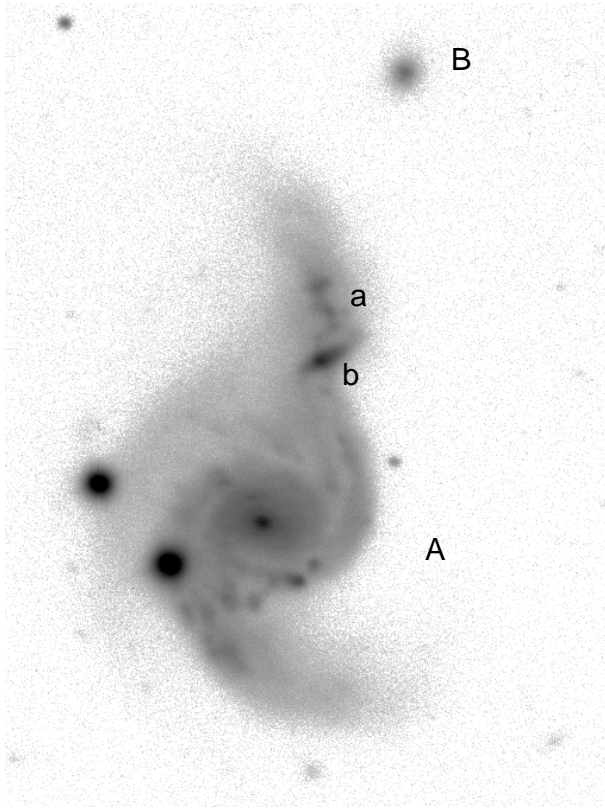
### 4.3. AM 0547-244

This system (Fig. 6) consists of a peculiar galaxy “A” ( $V_A = 13164 \text{ km s}^{-1}$ ), from which three tidal tails emanate, and a companion “B”, the redshift of which is unknown. The colors of the nuclei of “A” and “B” are very red (see Fig. 7). This could indicate an ‘old’ burst age or strong reddening due to large amounts of dust.

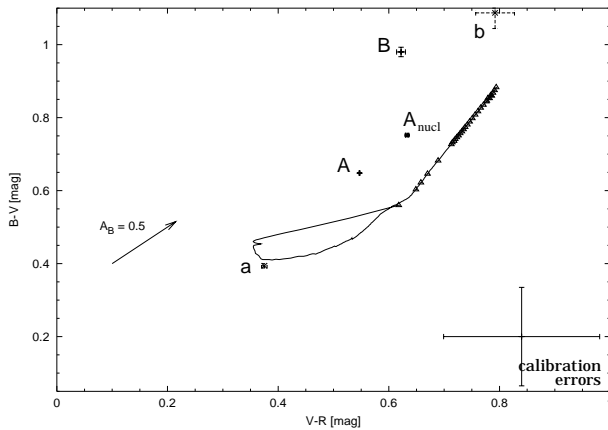
At the ends of the tails of galaxy “A” two large condensations are visible, denoted by “a” and “b”. With absolute magnitudes of  $M_{B_a} = -16.94$  and  $M_{B_b} = -17.05$ , “a” and “b” are good candidates for luminous TDGs. Around “A” four more knots with unknown redshift can be seen (“c” to “f”). All other objects have very red colors and are therefore most probably background objects.

Fig. 7 shows that the objects “a” to “d” agree well with the models with metallicity  $Z_1$  and intermediate to high burst strengths while “f” is not matched by any model. The interpretation of “a” to “f” is severely limited by the large systematic





**Fig. 8.** Identification chart of field 4 around AM 0607-444.



**Fig. 9.** Plot of the objects in field 4 of AM 0607-444. The model used is  $1(Z_1)$  (solid)  $b = 0.01$ .

errors of this field. A  $Z_3$  metallicity model can therefore not be excluded.

#### 4.4. AM 0607-444

This system consists of a spiral galaxy (“A”) which is severely disturbed in its outer parts (Fig. 8). The object labeled “B” has red colors and may be a background galaxy. Two objects are seen towards the northern tail. The very blue knot at its tip, “a”, hosts a star-forming region. In contrast, “b” is much redder, has elliptical contours in its center and may either be the remnant

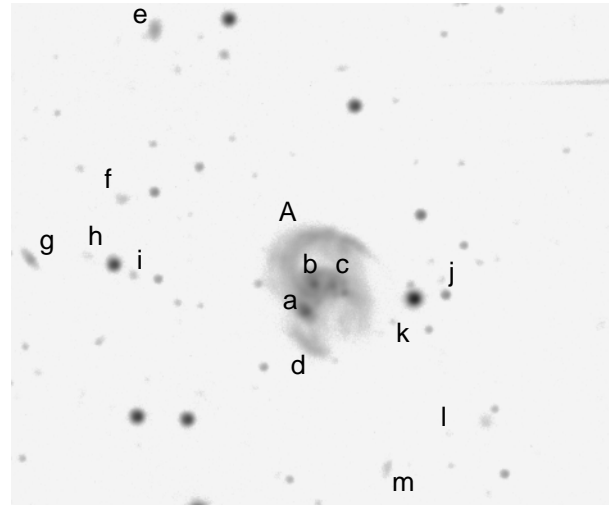


**Fig. 10.** Identification chart of field 5 around AM 0642-645.

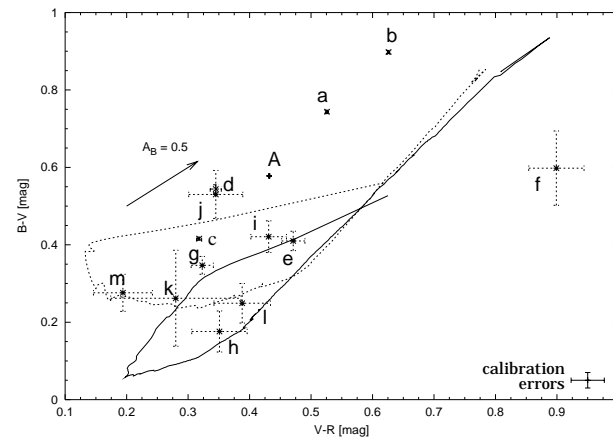


**Fig. 11.** Plot of the objects in field 5 of AM 0642-645. The models used are  $2(Z_1)$  (dotted,  $b = 0.05$ ) and  $5(Z_3)$  (solid,  $b = 0.09$ ).

core of the interacting companion of “A” or a background galaxy superimposed on the tail. The colors of the TDG candidate “a” are best matched with a  $Z_1$  model with a weak burst (Fig. 9), note, however, the large systematic errors of this field.

#### 4.5. AM 0642-645

The peculiar system “A” (Fig. 10) exhibits two red nuclei (“a”, “b”) and a bluer central knot, “c”, and may well be a merger. A plume to the southeast is designated with “d” and nine other extended objects in the field of view that have colors in the range of our models have been labeled. Fig. 11 shows that all of these objects would be consistent with TDG models having weak to intermediate burst strengths with the exception of object “f”, which has colors similar to an elliptical galaxy at  $z \approx 1.3$  (Möller et al. in prep.). However, without a spectroscopic redshift and in the absence of tidal structures linking them with the parent galaxy, the tidal origin of the objects surrounding “A” is very speculative.



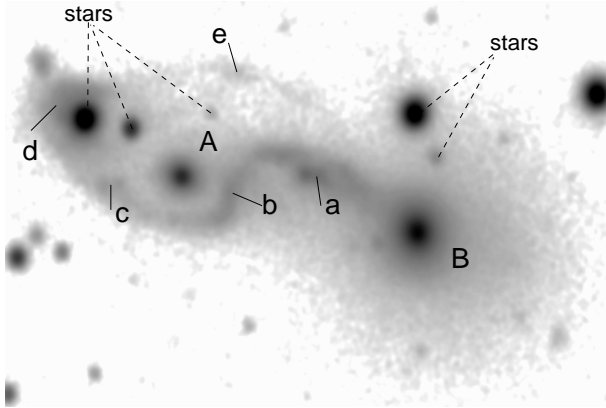


**Fig. 12.** Identification chart of field 6 around AM 0748-665.

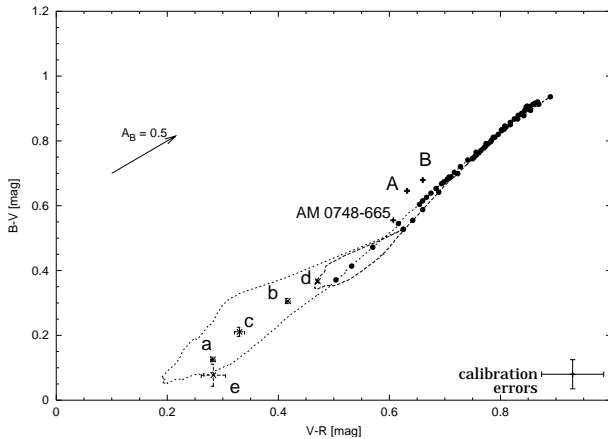


**Fig. 13.** Plot of the objects in field 6 of AM 0748-665. The models used are  $1(Z_3)$  (dashed) and  $3(Z_3)$  (dotted) with  $b = 0.01, 0.10$ .

#### 4.6. AM 0748-665

This interacting system is composed of two galaxies (“A” and “B”) which are connected by a long narrow bridge (Fig. 12). Their morphology indicates that the progenitors of “A” and “B” may have been a spiral and an elliptical, respectively. Several condensations labeled “a” to “e” can be seen in the associated tidal features. The brightest condensation “d” is blended with a bright star. The latter has been subtracted with a scaled PSF before carrying out the photometry. Fig. 13 shows that all data points agree with  $Z_3$  models that provide burst strengths up to 0.10.

#### 4.7. AM 1054-325

This presumably interacting system (Fig. 14) is composed of an irregular H II-galaxy, “A”, at a redshift of  $V_A = 3795 \text{ km s}^{-1}$  (Sekiguchi & Wolstencroft 1993) and a spiral-like object “B”, which has however colors that are redder and more homogeneous than typical spiral galaxies. Its redshift is not known. Object “C” is a LSB galaxy at an unknown redshift.

The enlarged image of “A” (Fig. 15) indicates that this galaxy seems to have two nuclei, one marked as “A<sub>nucl</sub>”, the other as “e” (blended by a foreground star). Like in AM 0529-565

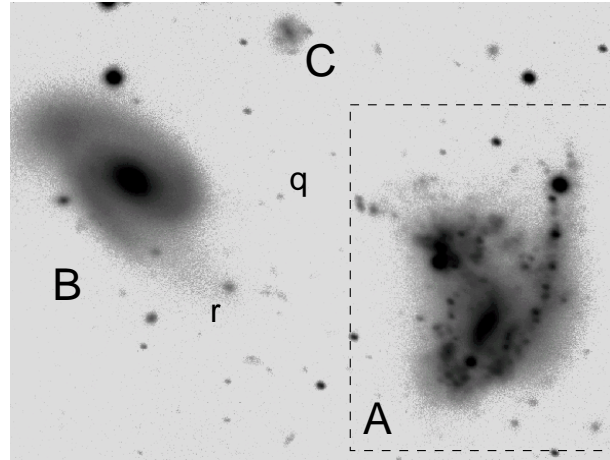


**Fig. 14.** Identification chart of field 7 around AM 1054-325.

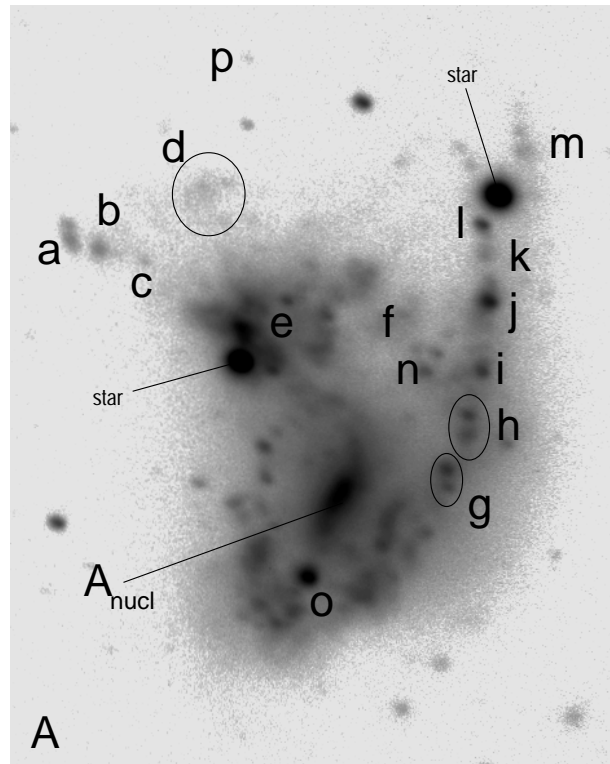


**Fig. 15.** Identification chart of AM 1054-325A.

A the two nuclei have different colors. The former is redder ( $B - V = 0.52$ ) while the latter has the blue colors of a strong starburst ( $B - V = 0.21$ ). Peña et al. (1991) derived for “A” an oxygen abundance of  $12 + \log(O/H) = 8.14$  equivalent to  $Z = 0.003$ . We therefore use our  $Z_1$  model for this galaxy.

In the western tail of “A” several large star-forming regions are visible (“g” to “m”) with luminosities of fainter dwarf galaxies. A few other features of special interest are marked as “a” to “d” and “f”. Fig. 16 shows that their colors are well matched with  $Z_1$  models with  $0.02 < b < 0.09$ . However “a”, “b” and “p” that have discrepant reddish colors are likely background

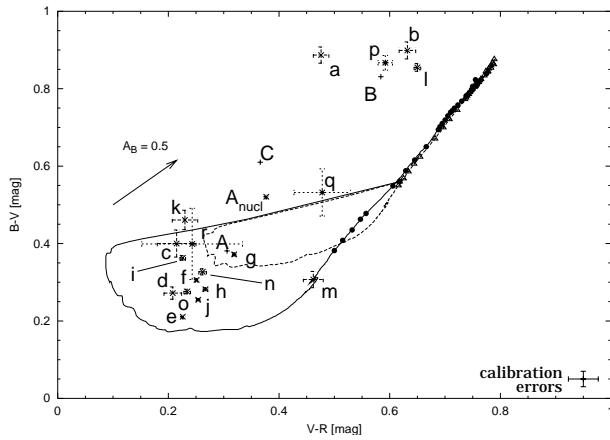


**Fig. 16.** Plot of the objects in field 7 of AM 1054-325. The models used are 4( $Z_1$ ) (dashed,  $b = 0.02$ ) and 5( $Z_1$ ) (solid,  $b = 0.09$ ).

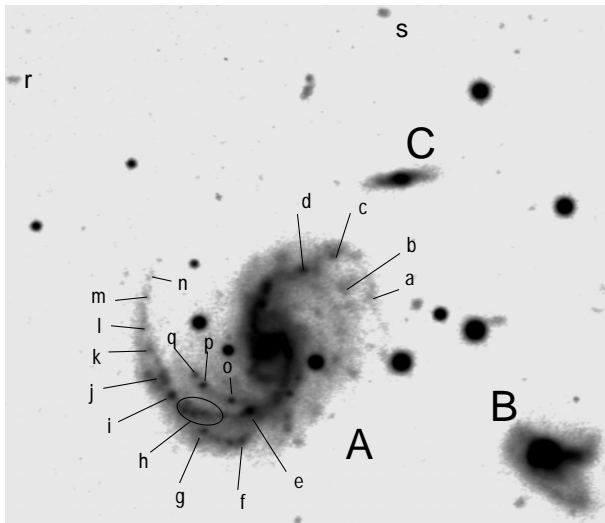


**Fig. 17.** Identification chart of field 8 around AM 1208-273.

objects. Note that the outlier “l” has a very uncertain photometry due to the vicinity of a bright saturated star.

#### 4.8. AM 1208-273

This system, also known as MCG-5-29-28, has three apparent members (Fig. 17). The main galaxy, “A”, is a disturbed Sc spiral with a small bar visible at the center ( $V_A = 14780 \text{ km s}^{-1}$ ). “B” is a foreground object with an active starburst ( $V_B = 12433 \text{ km s}^{-1}$ , Donzelli & Pastoriza 1997). The redshift of the disk galaxy “C” is not known.

Along the extended spiral arms of “A” several knots are visible, marked as “a” to “q”. Two detached diffuse objects “r” and “s” are visible northeast and north of the main galaxy, but their association with the other galaxies is uncertain. Fig. 18 shows that all knots in the arms are matched by a  $Z_3$  model with a high burst strength. They have roughly the same burst age.

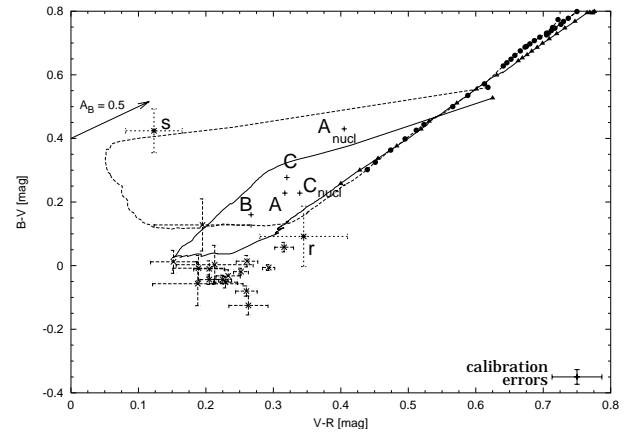


**Fig. 18.** Plot of the objects in field 8 of AM 1208-273. The models used are 6( $Z_1$ ) (dashed) and 6( $Z_3$ ) (solid) both with  $b = 0.18$ .

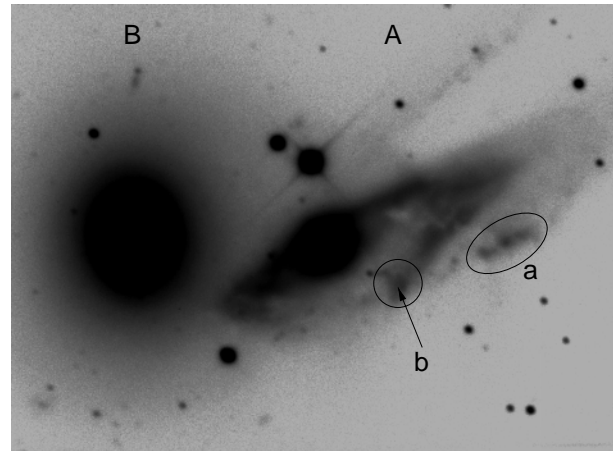


**Fig. 19.** Identification chart of field 9 around AM 1325-292.

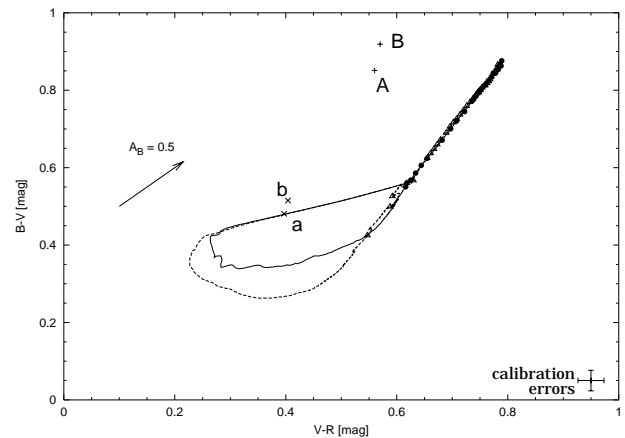


**Fig. 20.** Plot of the objects in field 9 of AM 1325-292. The models used are 4( $Z_1$ ) (solid,  $b = 0.02$ ) and 7( $Z_1$ ) (dashed,  $b = 0.04$ ).

#### 4.9. AM 1325-292

AM 1325-292 (Fig. 19) is a close interacting system between a spiral, NGC 5152 (“A”) and an elliptical, NGC 5153 (“B”). Their redshifts are  $V_A = 4598 \text{ km s}^{-1}$  and  $V_B = 4431 \text{ km s}^{-1}$ , respectively.

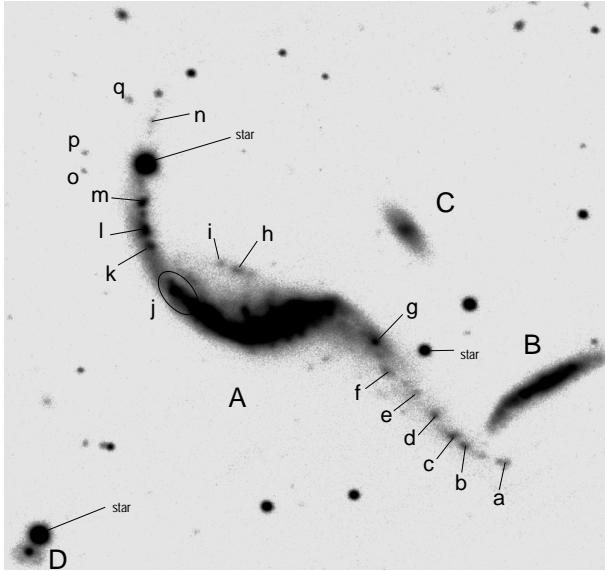


Fig. 21. Identification chart of field 10 around AM 1353-272.

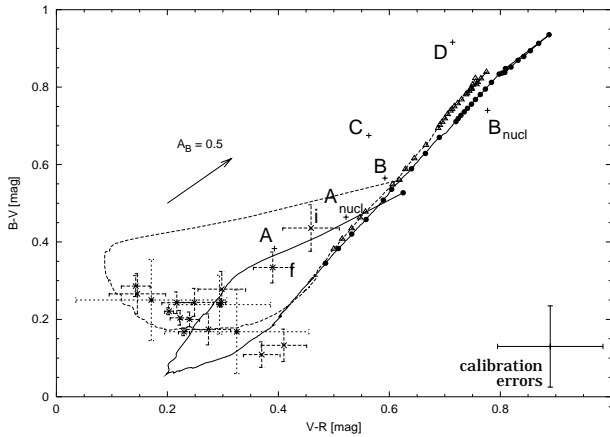


Fig. 22. Plot of the objects in field 10 of AM 1353-272. The models used are  $4(Z_1)$  (dashed,  $b = 0.02$ ) and  $6(Z_3)$  (solid,  $b = 0.18$ ).

The spiral has three visible spiral arms/tidal tails, a long one to the north and two apparently shorter ones to the southwest, at the end of which two bigger knots of dwarf galaxy size are seen (“a” and “b”). These knots have the bluest colors of the entire system and do well agree with  $Z_1$  models and small or intermediate burst strength shown in Fig. 20. The small photometric errors preclude  $Z_3$  models although due to the nature of the parent galaxy a higher metallicity would have been expected.

#### 4.10. AM 1353-272

Four galaxies are seen in the field of AM 1353-272 (Fig. 21). The two brightest are at the same redshift. “A” is an integral-sign spiral ( $V_A = 12145 \text{ km s}^{-1}$ ) interacting with a disturbed disk galaxy “B” ( $V_B = 11791 \text{ km s}^{-1}$ ). “C” is most probably a background elliptical, as judged from its red colors. “D”, to the southeast, is a LSB galaxy. Its color is highly uncertain due to the contamination by a bright foreground star.

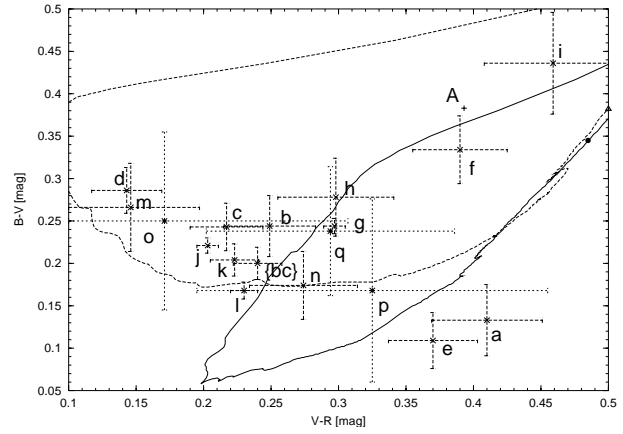


Fig. 23. Close-up of Fig. 22. The knots are now labeled.

The long tidal tails of “A” host a number of blue knots (“a” to “n”). Three detached small knots (“o” to “q”) are visible east of the northeast tail. Given their colors, these knots could be physically linked with “A” but without redshift information available this remains speculative. The knots have absolute magnitudes in the range of  $-12.1 < M_B < -15.7 \text{ mag}$ . Their colors do agree with the  $Z_3$  models and intermediate strength burst. Condensations “d” and “m” have however deviant colors that seem more consistent with  $Z_1$  models.

## 5. Discussion

### 5.1. Background contamination

In each field a number of faint extended objects are visible (see e.g. Figs. 4 and 6) that have red colors. They lie outside the color range of our models that are valid for  $z = 0$  only. Most of them should hence be background objects. This was tested using the chemically consistent evolutionary synthesis models of Möller et al. (1998) and Möller et al. (in prep.), which include cosmological parameters and give colors of all galaxy types as a function of  $z$ . A rough photometric redshift could be determined from the  $B, V, R$  measurements. The few faint objects with colors that strongly deviate from our TDG models and that are inconsistent with those of distant galaxies could be red dwarf galaxies pre-existing the collisions. They have been excluded from our analysis. One SUSI field with an area of  $1.3 \cdot 10^{-3} \text{ } \square^\circ$  contains on average  $7.0 \pm 0.7$  and  $13.0 \pm 4.0$  objects with deviant colors in the respective magnitude ranges  $B = 22 \dots 23$  and  $B = 23 \dots 24$ . After correction for the occlusion of background objects due to the interacting system (typically  $2 \cdot 10^{-4} \text{ } \square^\circ$ ), these values are compatible with those of Metcalfe et al. (1991). They imaged 12 fields with an area of  $6.8 \cdot 10^{-3} \text{ } \square^\circ$  and counted  $5000 \pm 800$  and  $15000 \pm 1000$  galaxies, respectively, for the magnitude ranges in question. For our field of view, the numbers would be  $6.8 \pm 1.1$  and  $20.2 \pm 1.3$ . Therefore we do not see an overdensity of background galaxies in our fields contrary to what Deeg et al. (1998) found in their sample of interacting systems. Their field of view is much larger (about  $3.3 \cdot 10^{-3} \text{ } \square^\circ$ ) than ours and they have better statis-

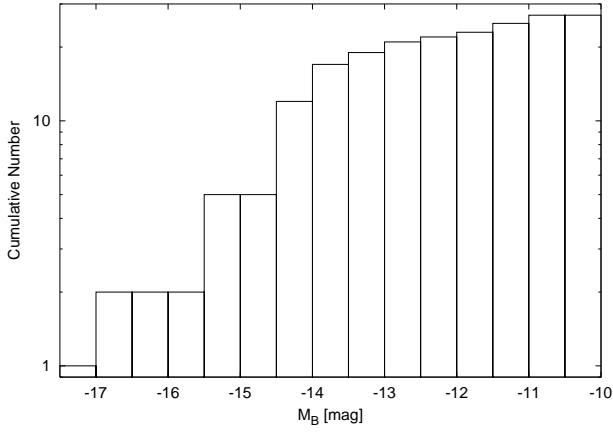


**Fig. 24.** Luminosity function of the tidal objects.

tics. But they mostly imaged interacting systems with lower  $z$  which hence occlude a larger portion of the image. Neither did they use color information to preselect possible nearby objects. Moreover, they mainly found an overdensity in the brightness range  $R = 18 \dots 19.5$  mag, where we do not have enough background objects for statistical analysis.

### 5.2. Properties of the TDG candidates

As seen before, several knots turn out to be background objects as judged from their colors. One should hence be cautious when physically linking faint objects with apparently nearby large galaxies. This is especially true for the detached objects lying far away from the tidal tails of the parent galaxies. In the absence of a redshift measurement, the color information and its comparison with the model predictions is useful to disentangle between possible objects in or close to tidal features from background galaxies. Using this technique, we have compiled a catalog of candidates for TDGs or their progenitors, i.e. knots associated with or close to tidal features that – within the observational errors – agree with one or more of our evolutionary synthesis models. They are listed in Table 4.

Column 1 shows the designation of the candidate. Column 2 gives, when its distance is known, the absolute blue magnitude of the TDG candidate. Columns 3 and 4 resp. give its  $B - V$  color and the difference in  $B - V$  between the knot and the surrounding tail (values in parentheses indicate detached knots). The last three columns list the results from the comparison with the models. Column 5 gives the ID of the best matching model(s), column 6 the most probable burst age(s), and column 7 a range of possible burst strengths. Note that the best-fit models shown here for every individual TDG candidate are not necessarily those shown in the plots in Sect. 4, where models were chosen to represent a maximum number of data points.

#### 5.2.1. Number and luminosity

In our sample of ten, 8 interacting systems contain promising TDG candidates. On average 3.6 were identified per system. The

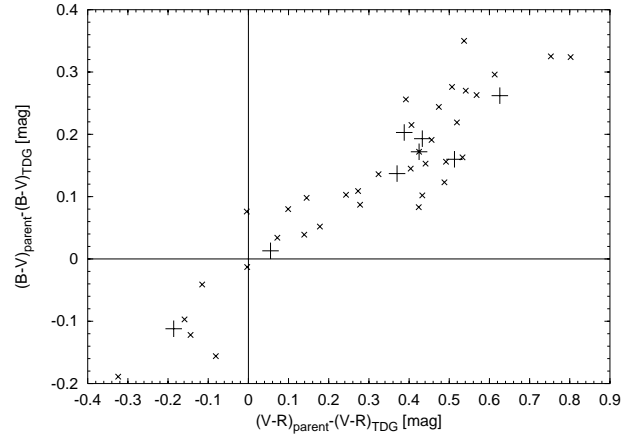


**Fig. 25.** Two-color-diagram of the differential colors of parent galaxies and TDG candidates. The small crosses mark the TDG candidates selected in Table 4. The big crosses mark the mean value of all TDG candidates in one given system.

luminosities of the candidates for which the distance of their parent galaxies is known range from faint ( $M_B = -10.4$  mag) to brighter dwarf galaxies ( $M_B = -17.1$  mag) with a mean of  $\langle M_B \rangle = -13.6$  mag. It should be noted that even though we have some faint TDG candidates in our sample, they are still more luminous than normal H II regions in spiral galaxies by about 4 mag (Bresolin & Kennicutt 1997). The luminosity function of the TDG candidates is shown in Fig. 24.

#### 5.2.2. Colors and star formation

In Fig. 25 we compare the colors of these knots with the overall colors of their parent galaxy. Note that the measurement of the parent galaxy includes the light of the knots, but this does not have a strong effect as the knots only give a negligible contribution (up to 1% of the flux) to the brightness of the galaxy.

On average the TDG candidates have bluer colors than their parent galaxies, which could be due to a number of effects:

- Fading effect: only the bluest clumps are visible. As we have selected the candidates from their surface brightness in the  $V$ -band images and all candidates have a young burst age, it is possible that after a longer burst the objects become redder and fade in luminosity and are no longer visible as surface brightness peaks in  $V$ .
- High relative gas content: the knots may experience stronger starbursts than the parent galaxies. A prerequisite for this could be a high gas content in the tidal features as observed in other systems (e.g. Duc & Mirabel 1998).
- Time difference: The burst in the parent galaxies may take place before the star formation in the tidal features starts. The color of the parent galaxy would then be dominated by the color of the red central part, especially after a strong nuclear starburst has faded.
- Smaller dust content: If the knots have a smaller dust extinction than the parent galaxies, their colors would appear redder.

**Table 4.** TDG candidates

Designation	$M_B$ [mag]	$B - V$ [mag]	$\Delta(B - V)$ (tail-TDG)	Best fit Model ID	burst age [Myr]	burst strength $b$
AM 0529-565a	-11.48	0.37	(0.03)	4( $Z_1$ )	4	0.02
AM 0529-565b	-10.65	0.52	(-0.12)	6( $Z_1$ )	<1	0.01..0.18
AM 0529-565g	-11.64	0.41	0.01	4( $Z_1$ )	3	0.02..0.05
AM 0529-565i	-12.57	0.42	0.15	6( $Z_1$ )	<1	0.05..0.18
AM 0537-292a		0.31	0.15	6( $Z_3$ )	1	0.04..0.18
AM 0537-292d		0.18	0.28	5( $Z_3$ )	10/3	0.05..0.18
AM 0537-292e		0.21	0.20	5( $Z_1$ )	8/3	0.09..0.18
AM 0537-292f		0.28	0.11	5( $Z_3$ )	$\approx 1$	0.05..0.10
AM 0537-292g		0.21	0.16	3( $Z_3$ )	10/3	0.09..0.18
AM 0547-244a	-16.94	0.34	0.07	9( $Z_1$ )	4	0.04..0.05
AM 0547-244b	-17.05	0.22	0.12	3( $Z_1$ )	<1..4	0.09..0.18
AM 0547-244d	-14.46	0.49	(-0.15)	6( $Z_1$ )	<1	0.02..0.18
AM 0607-444a		0.39	0.34	1( $Z_1$ )	<1/6	0.01..0.18
AM 0748-665a		0.13	0.32	2( $Z_3$ )	3/10	0.05
AM 0748-665d		0.21	0.11 <sup>1</sup>	1( $Z_3$ )	20	0.01
AM 0748-665e		0.08	0.15	3( $Z_3$ )	10	0.05..0.18
AM 1054-325g	-14.29	0.37	0.08	4( $Z_1$ )	5	0.02
AM 1054-325h	-13.73	0.28	0.11	7( $Z_1$ )	6	0.04
AM 1054-325i	-13.25	0.36	-0.02	7( $Z_1$ )	4	0.04
AM 1054-325j	-14.36	0.26	0.12	2( $Z_1$ )	6	0.05
AM 1054-325k	-10.40	0.46	-0.14	6( $Z_1$ )	<1	0.05..0.18
AM 1054-325m	-11.40	0.31	0.08 <sup>1</sup>	5( $Z_1$ )	70	0.05..0.18
AM 1325-292a	-15.30	0.48	0.15	5( $Z_1$ )	<1	0.01..0.18
AM 1325-292b	-15.46	0.52	0.18	6( $Z_1$ )	<1	0.01..0.18
AM 1353-272a	-13.68	0.13	(0.19)	7( $Z_3$ )	40	0.04..0.10
AM 1353-272b	-13.10	0.24	0.07	2( $Z_3$ )	9/3	0.04..0.18
AM 1353-272c	-13.58	0.24	0.02	2( $Z_3$ )	8	0.05
AM 1353-272d	-13.98	0.29	0.10	2( $Z_1$ )	4	0.05
AM 1353-272e	-14.03	0.11	0.27	5( $Z_3$ )	30	0.05..0.10
AM 1353-272f	-12.84	0.33	0.05	4( $Z_3$ )	<1/20	0.02..0.18
AM 1353-272h	-14.01	0.34	0.21	6( $Z_3$ )	2/10	0.04..0.18
AM 1353-272i	-12.13	0.44	0.04	1( $Z_3$ )	<1/40	0.01..0.18
AM 1353-272k	-13.99	0.20	0.11	5( $Z_1$ )/6( $Z_3$ )	8/3	0.05..0.18
AM 1353-272l	-15.25	0.17	0.12	5( $Z_1$ )/6( $Z_3$ )	9/3	0.09..0.18
AM 1353-272m	-14.49	0.14	0.03	2( $Z_1$ )	4	0.05..0.10
AM 1353-272n	-14.31	0.17	0.13	2( $Z_3$ )	10/3	0.05..0.10

<sup>1</sup> Contamination by a nearby bright star.

- The colors of the parent galaxies are largely dominated by the colors of their nuclei which are usually redder than the disk from which a TDG may form.

In order to tackle the last bias, we have compared the colors of the knots with the color of their immediate surroundings, i.e. in the tails. For knots already detached from the visible tail, the nearest part of the tail was taken for the measurement. The results are shown in Table 4, column 4 and in Fig. 26. Nearly all knots have a  $B - V$  color bluer than their surrounding tidal features. We therefore conclude that the knots are actively forming stars while their surrounding material is more quiescent.

As already noticed by Schombert et al. (1990), the tidal features and especially the surface brightness peaks which we identify as TDG candidates often show the bluest  $B - V$  colors of the entire interacting system.

Some examples of interacting galaxies show star formation in the tails but already have postburst characteristics in the central part of the merger (e.g. Hibbard et al. 1994). One could therefore conclude that star formation propagates from the central part to the outer regions along the tails and look for such an effect in interacting systems with several condensations along the tails. We do not find, however, any clear trends in the properties of the knots along the tails in the two systems which have longer tails (AM 1054-325A and AM 1353-272A) neither in luminosity or color, nor in burst strength or burst age.

### 5.2.3. Burst properties

The model bursts developed in this study that best fit the TDG candidates require intermediate to strong burst strength

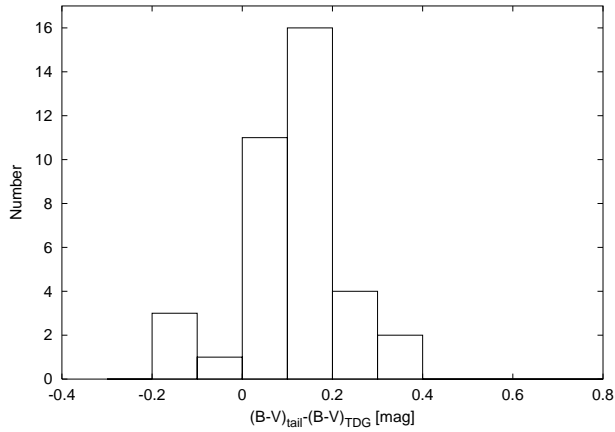


**Fig. 26.** Histograms of the differential colors of tidal features and the TDG candidates in  $B - V$ .

( $0.01 < b < 0.18$ ). Taking into account possible internal extinction would favor even stronger bursts. These burst strengths therefore seem to be higher than for BCDGs, which have typical strengths of  $b \approx 0.01$  or less (Krüger 1992). The burst strengths of our TDG candidates also indicate that the mass is still governed by the old stars ( $b < 0.20$ ), but the luminosities in  $B$  and  $R$  are already dominated by the young component (see Table 2).

The mean burst age of the tidal objects is about 8 Myrs. Their dynamical timescale may be determined assuming a typical distance of the knots from the nucleus of the parent galaxy of 15 kpc – about half of the length of the tails of AM 1353-272 – and a typical rotation velocity in a spiral galaxy of  $150 \text{ km s}^{-1}$ . With these values, disk material is expelled to the present positions of the knots in about 100 Myrs. Only very few objects in our sample show comparable high burst ages. This suggests that the star formation episode in the TDG candidates has started in situ in the tidally expelled material.

### 5.3. Nature of the TDG candidates

The condensations in the tidal tails which we call “Tidal Dwarf Galaxy candidates” show properties in the range expected for TDGs. We call them *candidates*, because they still lack spectroscopic confirmation and especially the proof that they are bound objects.

The TDG candidates identified in the systems presented here are on average less luminous but more numerous than the TDGs found in other interacting systems studied up to now. These other TDGs have an absolute blue magnitude of  $-15.5 \text{ mag}$  on average, part of them have been found to be kinematically decoupled from their tails (Duc et al. 1997; Duc & Mirabel 1998), and one or two of them are produced per collision. Moreover, the TDGs known to be gravitationally bound are found at the tip of the optical tails whereas our TDG candidates are distributed all along the tidal features without any trend in luminosity in agreement with one of the models discussed above. One reason for these differences may lie in the morphologies of the parent galaxies. TDGs have so far essentially been observed in merging systems involving massive spirals. Some of the interacting systems pre-

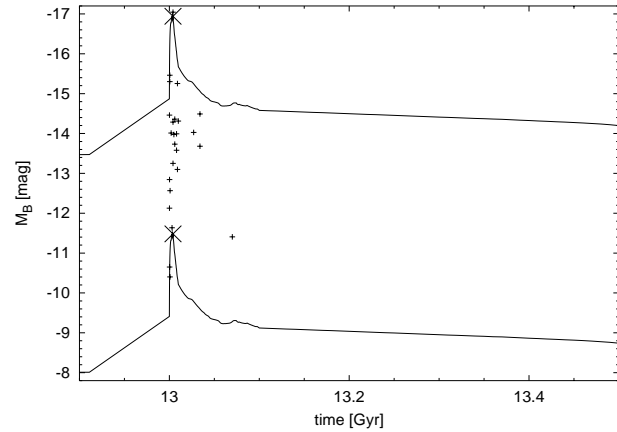


**Fig. 27.** Luminosity evolution of the selected TDG candidates which are displayed as crosses according to their luminosity and burst age. The models shown are 06( $Z_1$ ) with  $b = 0.18$  shifted in  $M_B$  to fit the two candidates represented by the larger crosses. See text about discussion of these two examples.

sented here are composed of late type galaxies, some of which have luminosities low enough to be classified as dwarf galaxies (e.g. AM 0529-565). It thus does not seem surprising that they form less massive condensations.

#### 5.3.1. Formation of bound objects

Numerical models of galaxy collisions show the presence of bound objects in tidal debris that have luminosities and distributions quite similar to the TDG candidates studied in our sample (e.g. Barnes & Hernquist 1992). The physical process for their formation is still largely unknown. They might either form from growing instabilities in the stellar component of tidal debris that may or may not attract surrounding gas (Barnes & Hernquist 1992), or alternatively from expelled gas that collapses and forms stars as proposed by Elmegreen et al. (1993). The blue colors of our TDG candidates favor the second scenario. Indeed we did not find any evidence for the presence of pure stellar condensations in the tidal features of our interacting systems. Our models show that recent star formation with a minimum strength of  $b \approx 0.01$ , i.e. forming 1% of young stars is necessary to account for the colors of our TDG candidates. In most cases, however, a much stronger burst is required. Note however, that we cannot distinguish between a stellar condensation into which gas falls later to cause the starburst and an initially gaseous condensation that forms stars on an underlying population of old stars.

#### 5.3.2. Future evolution

The spectrophotometric models are also used to extrapolate the evolution of the knots, i.e. to predict how luminosities and colors will change with time. The latter is already visible on the two-color diagrams in Sect. 4, where the evolution is marked in steps of 100 Myr along the model curves. Typically one Gyr after the burst, the optical colors of the condensations will be-

come indistinguishable from the pre-burst colors unless further star formation episodes take place. The luminosity evolution is shown in Fig. 27, where models for one of the most luminous TDG candidates, AM 0547-244a, and one of the least luminous candidates, AM 0529-565a, are displayed. Without secondary bursts, the  $B$ -luminosity will decrease by about 2.5 mag within 200 Myr from the present age. AM 0529-565a, with a present day absolute magnitude of  $M_B = -11.48$ , will fade to  $M_B \approx -8.0$  mag within 2 Gyrs. It will then have a luminosity similar to those of the faintest known galaxies of the local group (Mateo 1998). It would become invisible in our images at the distance of AM 0529-565. On a similar timescale, the more luminous TDG candidate AM 0547-244a ( $M_B = -16.94$ ) will fade to  $M_B \approx -13.4$  mag. It would be among the brighter dwarfs in the local group and could still be observed at its actual distance ( $m_B \approx 22.8$  mag).

The formation of objects as massive as TDGs in tidal debris is still puzzling. One may wonder whether the numerous knots that we observe here and that are produced in numerical simulations of galaxy collisions could be the progenitors of the more massive TDGs identified before. As the photometric models indicate a rapid fading of the TDGs after the burst, the evolution of a TDG progenitor into a TDG would require that star formation in these condensations is sustained for at least 100 Myrs, supposing that the progenitors initially have a large enough gas reservoir. TDG progenitors could grow that way and reach masses and luminosities of the well known TDGs. On the other hand, by that time, some of the less active TDG progenitors might have faded and those initially situated close to their parent galaxies might have fallen back, explaining why classical TDGs are found preferentially at the end of tidal tails. Observations of a larger sample of systems and more detailed simulations would be necessary to confirm the link between our TDG candidates and more luminous TDGs.

Another possibility is that the TDG candidates in this paper do not evolve into larger TDGs. Instead some of our TDG candidates may not grow much and eventually form more fragile TDGs of lower luminosity. Even if fading after the burst is taken into account, our faintest TDG candidates still have luminosities comparable to those of faint local group dwarf galaxies. The question if they will be able to survive as bound and dynamically independent objects can only be answered by observations of the kinematics in combination with detailed dynamical models.

To be able to do more than speculate about the dynamical fate of the TDG candidates, kinematical data of the system and the mass of the gaseous component of each knot is required. To further restrict the mass of the underlying old component NIR observations will be needed.

## 6. Conclusions

We have presented imaging data of 10 southern interacting systems from the Arp & Madore Catalog selected for their resemblance to disturbed distant galaxies. Our high quality images reveal a heterogeneous set of morphologies from loosely interacting dwarf galaxies to disk-disk mergers. Through detailed

photometry based on polygonal apertures in the three optical bands  $B, V, R$  we were able to measure the colors of about one hundred condensations in or near the tidal features of the interacting galaxies.

We have computed a grid of evolutionary synthesis models simulating starbursts of various strengths in an underlying stellar population of mixed ages typical of spiral galaxies. Such models reproduce well the situation of TDGs and their progenitors that are composed of an old population pulled out from the parent galaxy and young stars formed in situ. Our models take into account the emission lines and the continuum from the photoionized gas with appropriate metallicities. Comparing our photometric data with these models, we selected 36 blue condensations as possible TDGs. Follow-up spectroscopy is required in some cases to assess their physical association with the interacting system.

We discussed the overall properties of the 36 TDG candidates, noting that they have luminosities brighter than H II regions in spiral galaxies and more typical for that of dwarf galaxies. Their color is much bluer than those of their parent galaxies and mostly bluer than the surrounding material in the tidal features. The contribution of young stars to their mass is at least 1% and may reach 20% or more for the most active condensations. In any case their  $B$ -band luminosity is dominated by this young population. The models also indicate that after the starburst when the young stars cease to be the dominating source the condensations may fade by up to 2.5 mag in  $B$  within 200 Myrs after the burst. Although the TDG candidates seem to have young burst ages, we did not find any case of condensations solely made of old stars from the parent galaxies although the formation of such objects is also predicted in numerical simulations.

Finally the TDG candidates studied here have properties different from those of the more massive TDGs typically found at the tip of giant tidal tails of nearby interacting systems. We discuss whether our TDG candidates could be progenitors of TDGs or a class of less luminous objects.

*Acknowledgements.* We wish to thank the team at the NTT who made most of the observations under difficult conditions. We also thank our referee, E. Brinks, for careful reading of the manuscript and useful comments, which improved the paper. This research has made use of the NASA/IPAC Extragalactic Database (NED) which is operated by the Jet Propulsion Laboratory, California Institute of Technology, under contract with the National Aeronautics and Space Administration. PMW acknowledges partial support from DFG grant FR 916/6-1.

## References

- Appleton P.N., Marston A.P., 1997, AJ 113, 201
- Arp H.C., Madore B.F., 1987, A Catalogue of Southern Peculiar Galaxies and Associations. Cambridge University Press, Cambridge
- Barnes J.E., Hernquist L., 1992, Nat 360, 715
- Bransford M.A., Appleton P.N., Marston A.P., Charmandaris V., 1998, AJ 116, 2757
- Bresolin F., Kennicutt Jr. R.C., 1997, AJ 113(3), 975
- Burki G., Rufener F., Burnet M., et al., 1995, The Messenger 80, 34



- Burstein D., Heiles C., 1982, *AJ* 87, 1165
- Charbonnel C., Meynet G., Maeder A., et al., 1993, *A&AS* 101, 415
- Charbonnel C., Meynet G., Maeder A., Schaerer D., 1996, *A&AS* 115, 339
- Conselice C., Bershadly M.A., Dickinson M., et al., 1998, *A&AS* 193, 7512
- Deeg H.J., Muñoz-Tuñón C., Tenorio-Tagle G., et al., 1998, *A&AS* 129, 455
- Donzelli C.J., Pastoriza M.G., 1997, *ApJS* 111, 181
- Duc P.-A., Mirabel I.F., 1994, *A&A* 289, 83
- Duc P.-A., Mirabel I.F., 1997, *The Messenger* 89, 14
- Duc P.-A., Mirabel I.F., 1998, *A&A* 333, 813
- Duc P.-A., Brinks E., Wink J.E., Mirabel I.F., 1997, *A&A* 326, 537
- Elmegreen B.G., Kaufman M., Thomasson M., 1993, *ApJ* 412, 90
- Ferguson A.M.N., Gallagher J.S., Wyse R.F.G., 1998, *AJ* 116, 673
- Fritze-v. Alvensleben U., Gerhard O.E., 1994a, *A&A* 285, 751
- Fritze-v. Alvensleben U., Gerhard O.E., 1994b, *A&A* 285, 775
- Fritze-v. Alvensleben U., Möller C.S., Duc P.-A., 1998, In: Thuan T.X., Balkowski C., Cayatte V., Trân Thanh Vân J. (eds.) *Dwarf Galaxies and Cosmology*. Editions Frontières
- Hibbard J.E., Mihos J.C., 1995, *AJ* 110, 140
- Hibbard J.E., Guhathakurta P., van Gorkom J.H., Schweizer F., 1994, *AJ* 107, 67
- Izotov Y.I., Thuan T.X., Lipovetsky V.A., 1994, *ApJ* 435, 647
- Krüger H., 1992, Ph.D. Thesis, Universität Göttingen, Shaker-Verlag, Aachen
- Krüger H., Fritze-v. Alvensleben U., Loose H.-H., 1995, *A&A* 303, 41
- Landolt A.U., 1992, *AJ* 104, 340
- Leitherer C., Heckman T.M., 1995, *ApJS* 96, 9
- Mateo M.L., 1998, *ARA&A* 36, 435
- Metcalfe N., Shanks T., Fong R., Jones L.R., 1991, *MNRAS* 249, 498
- Mirabel I.F., Lutz D., Maza J., 1991, *A&A* 243, 367
- Möller C., Fritze-v. Alvensleben U., Fricke K.J., 1998, In: Guiderdoni B., Bouchet F.R., Thuan T.X., Tran Thanh Van J. (eds.) *The Birth of Galaxies*. Editions Frontières, in press
- Peña M., Ruiz M.T., Maza J., 1991, *A&A* 251, 417
- Savage B.D., Mathis J.S., 1979, *ARA&A* 17, 73
- Scalo J.M., 1986, *Fund. Cosmic Phys.* 11, 1
- Schaerer D., de Koter A., 1997, *A&A* 322, 598
- Schaerer D., Charbonnel C., Meynet G., et al., 1993a, *A&AS* 102, 339
- Schaerer D., Meynet G., Maeder A., Schaller G., 1993b, *A&AS* 98, 523
- Schaller G., Schaerer D., Meynet G., Maeder A., 1992, *A&AS* 96, 269
- Schombert J.M., Wallin J.F., Struck-Marcell C., 1990, *AJ* 99, 497
- Sekiguchi K., Wolstencroft R.D., 1993, *MNRAS* 263, 349
- Stasińska G., 1984, *A&AS* 55, 15
- van den Bergh S., Abraham R.G., Ellis R.S., et al., 1996, *AJ* 112, 359
- Zaritsky D., Kennicutt Jr. R.C., Huchra J.P., 1994, *ApJ* 420, 87